Mechanism of 8-Amino-7-oxononanoate Synthase: Spectroscopic, Kinetic, and Crystallographic Studies†,‡

ARTICLE *in* BIOCHEMISTRY · DECEMBER 1999

Impact Factor: 3.02 · DOI: 10.1021/bi991620j

Mechanism of 8-Amino-7-oxononanoate Synthase: Spectroscopic, Kinetic, and Crystallographic Studies[†,‡]

Scott P. Webster,[§] Dmitriy Alexeev,[||] Dominic J. Campopiano,[§] Rory M. Watt,[§] Marina Alexeeva,[§] Lindsay Sawyer,*[,||] and Robert L. Baxter*[,§]

Edinburgh Centre for Protein Technology, Department of Chemistry, University of Edinburgh, King's Buildings, West Mains Road, Edinburgh EH9 3JJ, United Kingdom, and Structural Biochemistry Group, ICMB, University of Edinburgh, Swann Building, King's Buildings, Mayfield Road, Edinburgh EH9 3JR, United Kingdom

Received July 14, 1999; Revised Manuscript Received October 25, 1999

ABSTRACT: 8-Amino-7-oxononanoate synthase (also known as 7-keto-8-aminopelargonate synthase, EC 2.3.1.47) is a pyridoxal 5′-phosphate-dependent enzyme which catalyzes the decarboxylative condensation of L-alanine with pimeloyl-CoA in a stereospecific manner to form 8(*S*)-amino-7-oxononanoate. This is the first committed step in biotin biosynthesis. The mechanism of *Escherichia coli* AONS has been investigated by spectroscopic, kinetic, and crystallographic techniques. The X-ray structure of the holoenzyme has been refined at a resolution of 1.7 Å (R = 18.6%, R_{free} = 21.2%) and shows that the plane of the imine bond of the internal aldimine deviates from the pyridine plane. The structure of the enzyme−product external aldimine complex has been refined at a resolution of 2.0 Å (R = 21.2%, R_{free} = 27.8%) and shows a rotation of the pyridine ring with respect to that in the internal aldimine, together with a significant conformational change of the C-terminal domain and subtle rearrangement of the active site hydrogen bonding. The first step in the reaction, L-alanine external aldimine formation, is rapid ($k_1 = 2 \times 10^4$ M^{-1} s^{-1}). Formation of an external aldimine with D-alanine, which is not a substrate, is significantly slower ($k_1 = 125$ M^{-1} s^{-1}). Binding of D-alanine to AONS is enhanced approximately 2-fold in the presence of pimeloyl-CoA. Significant substrate quinonoid formation only occurs upon addition of pimeloyl-CoA to the preformed L-alanine external aldimine complex and is preceded by a distinct lag phase (∼30 ms) which suggests that binding of the pimeloyl-CoA causes a conformational transition of the enzyme external aldimine complex. This transition, which is inferred by modeling to require a rotation around the Cα−N bond of the external aldimine complex, promotes abstraction of the Cα proton by Lys236. These results have been combined to form a detailed mechanistic pathway for AONS catalysis which may be applied to the other members of the α-oxoamine synthase subfamily.

Biotin is an essential enzyme cofactor for carboxylase and transcarboxlase reactions. The biosynthesis of biotin appears to follow similar pathways in both plants and microorganisms, and thus, inhibition of the enzymes involved in the pathway is potentially an attractive target for both herbicide and antibiotic development. In *Escherichia coli*, biosynthesis of biotin is catalyzed by the products of four genes (*bio*A, *bio*B, *bio*D, and *bio*F). The product of the *bio*F gene, 8-amino-7-oxononanoate synthase (AONS,[1] EC 2.3.1.47), is a PLP-dependent enzyme which catalyzes the first committed step of the pathway in *E. coli* (*1*). This involves the decarboxylative condensation of pimeloyl-CoA and L-alanine to produce AON, coenzyme A, and carbon dioxide (Figure 1).

The structure and reaction mechanism of AONS places it in the α-family of PLP-dependent enzymes (*2*−*4*). Comparison of the AONS tertiary structure with those of other PLP-dependent enzymes has shown that it is structurally closely related to dialkylglycine decarboxylase, a type II aminotransferase (*5*). Alignment of the amino acid sequence of AONS with the other three enzymes of the α-oxoamine synthase family (5-aminolevulinate synthase, serine palmitoyltransferase, and 2-amino-3-oxobutyrate CoA ligase) shows that almost all of the active site residues are conserved within this family of enzymes (*6*). Recent studies have shown that in AONS, the only member of the α-oxoamine synthase family for which a structure has been determined, the PLP cofactor is covalently bound to Lys236 through an imine (Schiff's base) linkage and interacts with

[†] This work was supported by the Biotechnology and Biological Sciences Research Council, U.K. (to L.S. and R.L.B.). R.M.W. was supported by a BBSRC/Zeneca Case award. We are thankful for the support under the TMR/LSF program to the EMBL/DESY outstation (ERBFMGECT980134).

[‡] The coordinates have been deposited in the Protein Data Bank [files IDJE (PLP form) and IDJ9 (AON−PLP form)].

* To whom correspondence should be addressed. R.L.B.: Edinburgh Centre for Protein Technology, Department of Chemistry, University of Edinburgh, King's Buildings, West Mains Road, Edinburgh EH9 3JJ, United Kingdom; telephone, +44 131 650 4708; fax, +44 131 650 7155; e-mail, R.Baxter@ed.ac.uk. L.S.: Structural Biochemistry Group, University of Edinburgh, Swann Building, King's Buildings, Mayfield Road, Edinburgh EH9 3JR, United Kingdom; telephone, +44 131 650 7062; fax, +44 131 650 7055; e-mail, L.Sawyer@ed.ac.uk.

[§] Edinburgh Centre for Protein Technology, Department of Chemistry, University of Edinburgh.

[||] Structural Biochemistry Group, ICMB, University of Edinburgh.

[1] Abbreviations: AONS, 8-amino-7-oxononanoate synthase; AON, 8-amino-7-oxononanoate; CoA, Coenzyme A.; PLP, pyridoxal 5′-phosphate; EDTA, ethylenediaminetetraacetate.

10.1021/bi991620j CCC: $19.00
Published on Web 12/22/1999

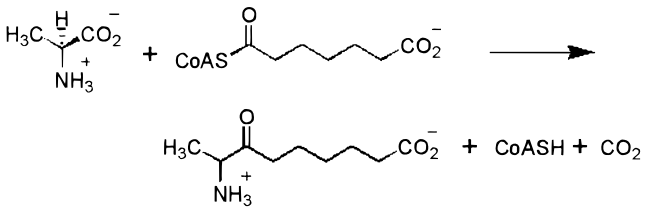

FIGURE 1: General reaction catalyzed by AONS.

two other basic residues, His133 and His207, which may play an important role in substrate binding and catalysis (*6*). The mechanism of AONS catalysis appears to be similar to those of other PLP-dependent enzymes (*7*). The initial steps of the reaction involve displacement of the internal aldimine complex by the incoming amino acid substrate to form an external aldimine, followed by heterolytic cleavage of a Cα bond of the amino acid. Several studies have indicated that the conserved active site lysine involved in PLP binding also acts as the catalytic base (*8*−*11*). In general, cleavage of a Cα bond leads to the generation of a resonance-stabilized quinonoid intermediate which may be observed spectroscopically (*12*−*15*). Although quinonoid formation from the alanine external aldimine of AONS has not been observed spectroscopically. However, the Cα−H of the L-alanine external aldimine has been shown to exchange with deuterium (from D_2O), indicating that the Cα−H bond (not the Cα−carboxylate bond) of the initial substrate external aldimine is cleaved to form the initial quinonoid intermediate (*16*). This quinonoid can be presumed to react subsequently with the other substrate, pimeloyl-CoA, in a Claisen-type condensation to form a putative β-ketoacid aldimine intermediate. The next step in the sequence is presumably decarboxylation of the resultant β-ketoacid. In *Bacillus sphaericus* AONS, the formation of a second quinonoid intermediate is indicated by the fact that C6 and C8 of AON are deuterated when the reaction is carried out in D_2O (*16*). Further incubation of mammalian 5-aminolevulinate synthase with its product (5-aminolevulinate) affords both an external aldimine complex and a stable quinonoid complex (*17*). Mutagenesis of the catalytic lysine in 5-aminolevulinate synthase results in loss of catalytic activity, suggesting that proton abstraction from the Cα position of the external aldimine complex is primarily mediated by the active site lysine, although abstraction of a proton from the product−enzyme complex could in principle also occur via a general base-catalyzed mechanism involving other basic active site residues (*18*). It is possible that the catalytic proton abstraction may be mediated by either of these active site histidine residues.

A more complete understanding of the complex reaction sequence catalyzed by these enzymes requires more detailed investigation of substrate, intermediate, and product complexes. Here we report spectroscopic and kinetic studies of the interaction of AONS with its substrates and product and the crystallographic characterization of the *E. coli* AONS−product external aldiimine complex which suggest the basis of a mechanistic pathway which may prove to be common to all four enzymes of the α-oxoamine synthase family.

EXPERIMENTAL PROCEDURES

Materials. Restriction endonucleases and DNA-modifying enzymes were obtained from Promega, New England Biolabs, and Pharmacia Biotech Inc. and used according to the manufacturer's instructions. The Prep-A-Gene kit (Bio-Rad) was used to isolate DNA fragments from restriction digests, PCR mixtures, and agarose gels. Plasmid purification was carried out using Promega "Wizard" miniprep kits. All other chemicals were analytical grade and were obtained from commercial sources.

Manipulation of DNA. DNA manipulations were generally performed using standard procedures for *E. coli* (*19*). Standard conditions were used for restriction endonuclease digestions, agarose gel electrophoresis, and DNA ligation reactions according to the manufacturer's instructions.

Purification of AONS. Expression of AONS was carried out as previously described and purified with the following modifications (*6*). Following ammonium sulfate fractionation, the protein was resuspended in the minimum volume of 20 mM potassium phosphate (pH 7.5) containing 2 mM EDTA and 100 μM PLP. The protein solution was adjusted to 20% (w/v) ammonium sulfate and loaded onto a phenyl-Sepharose column (Pharmacia) pre-equilibrated with 20 mM potassium phosphate buffer (pH 7.5) containing 20% (w/v) ammonium sulfate, 2 mM EDTA, and 100 μM PLP. The protein was eluted with a linear gradient [20 → 0% (w/v) ammonium sulfate in buffer] over 10 column volumes. Fractions containing AONS were pooled and loaded onto a Q-Sepharose anion exchange column (Pharmacia) pre-equilibrated with 20 μM potassium phosphate (pH 7.5) containing 2 mM EDTA and 100 μM PLP. The pure protein was eluted with a linear salt gradient (0 → 1 M NaCl) over 20 column volumes. The protein fractions were analyzed by SDS−PAGE, and the concentration of AONS was quantified using the method of Bradford using BSA as a standard (*20*). The enzyme was stored at −20 °C in 20 mM potassium phosphate (pH 7.5) containing 100 μM PLP and 20% (v/v) glycerol.

N-Terminal Sequencing. The N-terminal sequence of the purified AONS protein was determined by gas-phase Edman degradation (WELMET Edinburgh Protein Characterisation Facility).

Mass Spectrometry. Electrospray mass spectrometry was performed on a Micromass Platform II quadrupole mass spectrometer equipped with an electrospray ion source. The cone voltage was set to 70 V and the source temperature to 95 °C. Protein samples [10 μg of AONS in 20 mM potassium phosphate (pH 7.5)] were separated on a Jupiter 5 μm C-4 300A column at a constant TFA concentration of 0.01% using a linear gradient of 10 to 100% acetonitrile in water over the course of 40 min at a flow rate of 0.05 mL/min. The total ion count of all the ions in the range of m/z 500−2000 and the UV chromatogram at 280 nm were recorded for the reversed-phase HPLC separation. The mass spectrometer was scanned at intervals of 0.1 s; the scans were collected and the spectra combined, and the average molecular mass was determined using the MaxEnt algorithm of MassLynx software.

Synthesis of Substrates. Pimeloyl-CoA was synthesized according to the method described previously (*21*). Pimeloyl-CoA was purified via reverse-phase HPLC through an Aquapore C8 column using a linear gradient of water/acetonitrile (10 to 100%) containing 0.1% TFA.

(±)-8-Amino-7-oxononanoate (AON) was synthesized by sequentially treating 2-acetyl-1,3-dithiolane with LDA (prepared in situ) and ethyl 6-iodohexanoate in THF/HMPA at

−78 °C to give ethyl 7,7-(ethylenedithio)-8-oxononanoate (*22*). This was reductively aminated using HMDS/$TiCl_4$/$NaCNBH_3$ (*23*). The resulting amine was deprotected using aqueous *N*-bromosuccinimide, and the reaction was quenched with aqueous HCl to give (±)-AON as its HCl salt in an overall yield of 26%. The product was further purified by cation exchange chromatography [Dowex 50X resin using a linear HCl gradient (0 to 1 M)] and finally crystallized as its HCl salt: NMR (D_2O, 200 MHz) δ_H 1.13−1.24 (2H, m, 4-CH_2), 1.39 (3H, d, J = 7.5 Hz, 9-CH_3), 1.35−1.53 (4H, m, 3- and 5-CH_2), 2.22 (2H, t, J = 7.3 Hz, 2-CH_2), 2.52 (2H, m, 6-CH_2), 4.10 (1H, q, J = 7.5 Hz, 8-CH); NMR (D_2O, 62.9 MHz) δ_C 14.6 (C-9), 22.2, 23.9 and 27.5 (C-3, -4, and -5), 33.7 (C-2), 37.8 (C-6), 54.8 (C-8), 179.0 (C-1), 209.3 (C-7); MS (FAB) MH^+ at *m*/*z* 188.12882, $C_9H_{18}NO_3$ requires 188.12867.

Assay of AONS Activity. AONS activity was determined using a linked assay by monitoring the increase in absorption of NADH at 340 nm using a Hewlett-Packard 8452A diode array spectrophotometer, thermostatically controlled at 30 °C. A typical assay contained 20 mM potassium phosphate (pH 7.5), 1 mM α-ketoglutarate, 0.25 mM thiamine pyrophosphate, 1 mM NAD^+, 3 mM $MgCl_2$, 0.1 unit of α-ketoglutarate dehydrogenase, and 2−10 μg of AONS in a total volume of 1 mL. L-Alanine and pimeloyl-CoA were added to give the desired final concentrations. Data were acquired using HP 89532K Multicell Kinetics software. Kinetic constants were determined from saturation curves in which the second substrate concentration was fixed. Data were fitted to a standard Michaelis curve using Microcal Origin software.

Spectroscopic Methods. All UV−visible spectra were recorded on a Hewlett-Packard 8452A diode array spectrophotometer. Prior to analysis, enzyme samples were dialyzed for 2 h at 4 °C against 20 mM potassium phosphate (pH 7.5) containing 100 μM PLP. The AONS concentration in all analyses was 10 μM in 20 mM potassium phosphate (pH 7.5). Reference cuvettes contained all other components except AONS.

Determination of Dissociation Constants. Enzyme samples were treated with 100 μM PLP in 20 mM potassium phosphate (pH 7.5). Non-enzyme-bound PLP was removed by gel filtration of the solution on a Sephadex G-25 column (Pharmacia) using 20 mM potassium phosphate (pH 7.5) as the eluent. Protein fractions were concentrated on a Centrex UF2 concentrator (Schleicher & Schuell). Assays were carried out in 1 mL quartz cuvettes and typically contained 10−50 μM AONS in 20 mM potassium phosphate (pH 7.5). Varying amounts of L- or D-alanine (0−80 mM) were used in each assay. Pimeloyl-CoA (143 μM) was also included in assays where required. After addition of substrate, the reactants were mixed and allowed to equilibrate for 20 min at 30 °C. Spectra were recorded on a Hewlett-Packard 8452A diode array spectrophotometer thermostated at 30 °C. Small baseline changes were corrected using Origin Software. Changes in absorbance at 425 nm were plotted against L- or D-alanine concentrations, and data points were fitted to a hyperbolic saturation curve (eq 1) using Origin software:

$$\Delta A_{obs} = \frac{\Delta A_{max}[\text{alanine}]}{K_d + [\text{alanine}]} \quad (1)$$

where ΔA_{max} is the maximal absorbance change, [alanine] is the L- or D-alanine concentration, and K_d is the dissociation constant.

Stopped-Flow Kinetics. Transient absorption kinetics were assessed under pseudo-first-order conditions. Spectra were recorded on an Applied Photophysics SX17 stopped-flow spectrophotometer, thermostatically controlled at 30 °C. For the determination of the rates of formation of external aldimine, syringes contained 20 μM AONS and 0−100 mM L- or D-alanine. Spectra were recorded at 425 nm and fitted to single-exponential saturation curves. Rate constants were determined from the slope of a best-fit line produced from a plot of observed rate versus alanine concentration. For analysis of substrate-induced quinonoid formation, one syringe contained 25 μM AONS pre-equilibrated with 10 mM L-alanine and the other 0−300 μM pimeloyl-CoA. Spectra were recorded at 486 nm and the separate phases fitted to single-exponential curves.

Crystallography. The crystals of AONS were grown from ammonium sulfate in space group $P3_112$ ($a = b = 58.22$ Å, $c = 194.83$ Å, and $\gamma = 120°$) as described previously (*6*). The crystals were presoaked overnight in well solution containing 10 mM fresh PLP to transform the enzyme into the PLP-bound active form. The crystals of the holoenzyme were frozen in liquid nitrogen and the diffraction data collected to a resolution of 1.7 Å (at beamline X11, EMBL/DESY, Hamburg, Germany).

AON was added to the well solution of the PLP-pre-equilibrated crystals of the holoenzyme at a final concentration of 100 μM, and the crystals were soaked for 2 h to achieve full binding of AON. The crystals were frozen in liquid nitrogen and the X-ray diffraction data collected to a resolution of 2.0 Å (at station 7.2 SRS, CLRC Daresbury Laboratory, Warrington, U.K.). The data were reduced with DENZO/SCALEPACK, and both structures were refined with SHELX97. The refinement calculation was interleaved with several rounds of model building with the program O. Water molecules were added using the program SHELX-WAT. The data collection and refinement details are summarized in Table 3. The Mg^{2+} ion was added to the model manually after all water molecules had been incorporated into the model.

RESULTS

Enzyme Characterization and Activity. Our original cloning, overexpression, and purification of *E. coli* AONS were briefly reported in an earlier publication (*6*). However, the method described here results in a greater yield of the homogeneous holoenzyme with a higher specific activity in only two chromatographic steps. The enzyme has been further characterized by N-terminal amino acid sequencing and mass spectrometry. The N-terminal sequence of the first five amino acid residues was determined to be SWQEK, indicating that the protein is post-translationally modified and lacks the N-terminal methionine. This result was confirmed by our X-ray study in which the protein sequence begins with residue Ser2. This contrasts with the N-terminus of the *B. sphaericus* enzyme expressed in *E. coli* which is unmodified (*21*). The sequencing data are in close agreement with the predicted mass. The observed mass of the holoenzyme is slightly higher than the predicted value, but this

Table 1: Electrospray Mass Spectrometry Data for *E. coli* AONS[a]

	apoenzyme	holoenzyme
predicted mass (Da)	41 463.1	41 694.1
measured mass (Da)	41 464.4 (4.5)	41 740.9 (6.1)

[a] Data were acquired as described in Experimental Procedures. Errors are given in parentheses.

Table 2: Comparison of Steady-State Rate Constants for AONS[a]

	pimeloyl-CoA			L-alanine	
AONS	k_{cat} (s^{-1})	K_m (μM)	k_{cat}/K_m (s^{-1} M^{-1})	K_m (mM)	k_{cat}/K_m (s^{-1} M^{-1})
E. coli	0.06 (0.01)	25 (2)	2400 (430)	0.50 (0.04)	120 (21)
B. sphaericus	0.3[b]	1.5[b]	2×10^5	2.5[b]	120

[a] Kinetic assays were carried out as described in Experimental Procedures. Errors are given in parentheses. To check for the requirement of a Mg^{2+} ion for catalysis, assays were also carried out in the presence of EDTA. The steady-state kinetic parameters were comparable to those determined in the absence of EDTA. [b] Data from O. Ploux (personal communication).

discrepancy can be rationalized if it assumed that two sodium ions become associated with the complex during mass spectrometric analysis (Table 1).

In our hands, we found the published assay for *B. sphaericus* AONS activity, which involves measuring the disappearance of the pimeloyl-CoA thioester bond absorbance at 230 nm, to be unreliable for the *E. coli* enzyme (*16*). Instead, we employed a coupled assay which relies upon monitoring the release of CoA from pimeloyl-CoA (*24*).

The kinetic constants obtained differ from those determined for the corresponding *B. sphaericus* enzyme (Table 2) (*16*, *21*). For the *E. coli* enzyme, the K_m values for L-alanine and pimeloyl-CoA are similar to those of other acyl-CoA condensing enzymes, which are typically in the millimolar range for the amino acid substrate and micromolar range for the CoA-derived substrate (*25*, *26*). The K_m determined for pimeloyl-CoA is slightly greater than that for the corresponding *B. sphaericus* enzyme, indicating that the *E. coli* enzyme has a lower specificity for pimeloyl-CoA. The *E. coli* enzyme is approximately 6 times slower than the *B. sphaericus* enzyme.

Distinct Absorbance Spectra Characterize the Reaction Intermediates. By monitoring the spectral changes induced by the interaction of AONS with its substrates and products, we were able to identify several of the intermediate species in the AONS catalytic pathway. The absorbance spectrum of AONS holoenzyme exhibits peaks at 334 and 425 nm which we assign to the non-coplanar and coplanar forms of the AONS−PLP internal aldimine complex (Figure 2). This spectrum is not affected by changes in monovalent metal ion or pH (data not shown). Addition of divalent metal ions (Ca^{2+}, Mg^{2+}, and Mn^{2+}) at low concentrations has no effect on the spectra. Higher concentrations (>10 mM) result in a slow precipitation of the protein.

The increase in the absorbance of the 425 nm band, on addition of L- and D-alanine to AONS (Figure 2A), indicates formation of an external aldimine (Figure 3, II). Further titration of AONS with increasing concentrations of L- or D-alanine does not, however, lead to quinonoid formation, which is usually manifested by a bands at longer wavelengths.

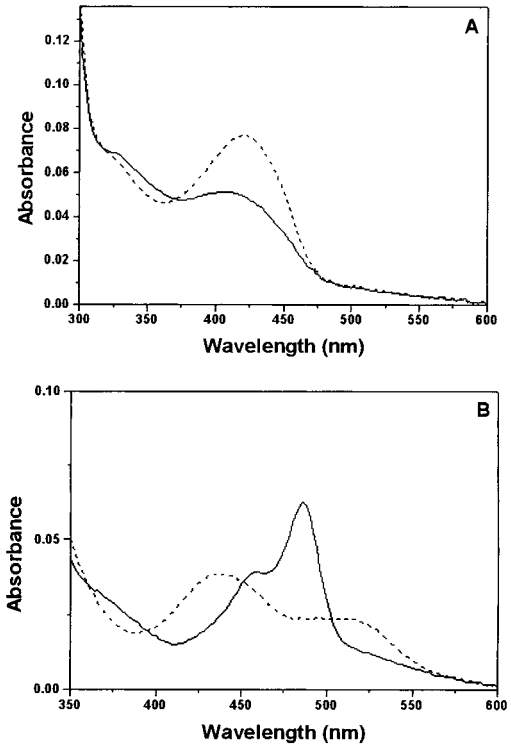

FIGURE 2: Changes in cofactor absorption spectra of AONS. Spectra were acquired at 25 °C and pH 7.5: (A) 10 μM AONS (solid line) and AONS in the presence of 10 mM L-alanine (dashed line) and (B) AONS in the presence of 10 mM L-alanine and 100 μM pimeloyl-CoA (solid line) and AONS in the presence of 2 mM (±)-AON (dashed line).

Addition of pimeloyl-CoA to the external aldimine form of the enzyme results in immediate formation of a band at 486 nm (Figure 2B and Figure 3, IV) which diminishes slowly over the course of several minutes. The formation of this band is dependent on pimeloyl-CoA concentration and is accompanied by the appearance of a shoulder at 460 nm (Figure 2B). The appearance of the 486 nm band strongly implies formation of a quinonoid species (Figure 3, IV), and it is noteworthy that this is only observed after addition of pimeloyl-CoA to the enzyme.

Incubation of the AONS holoenzyme with the product of the reaction, AON, gives rise to a spectrum with maxima at 436 and 520 nm (Figure 2B). It seems likely that these bands correspond to the formation of product external aldimine and its quinonoid (Figure 3, VII and VI, respectively). We have assigned the wavelength of the broad quinonoid band as 520 nm, although it is possible that the true maximum may be at a slightly shorter wavelength. It is also interesting to note that the quinonoid form of the product−PLP complex has an absorption maximum at a substantially longer wavelength than the substrate−PLP quinonoid formed earlier in the catalytic pathway.

Interaction with L- and D-Alanine. The increase in the external aldimine concentration was determined by measuring the change in absorbance at 425 nm in the presence of varying amounts of L- or D-alanine. Plots of absorption increase at 425 nm versus L-alanine concentration gave a curve with a dissociation constant K_d of 0.9 mM (Figure 4). Titration of AONS with D-alanine gave a K_d of 9.8 mM, while titration of D-alanine in the presence of saturating amounts of pimeloyl-CoA led to a more than 2-fold decrease

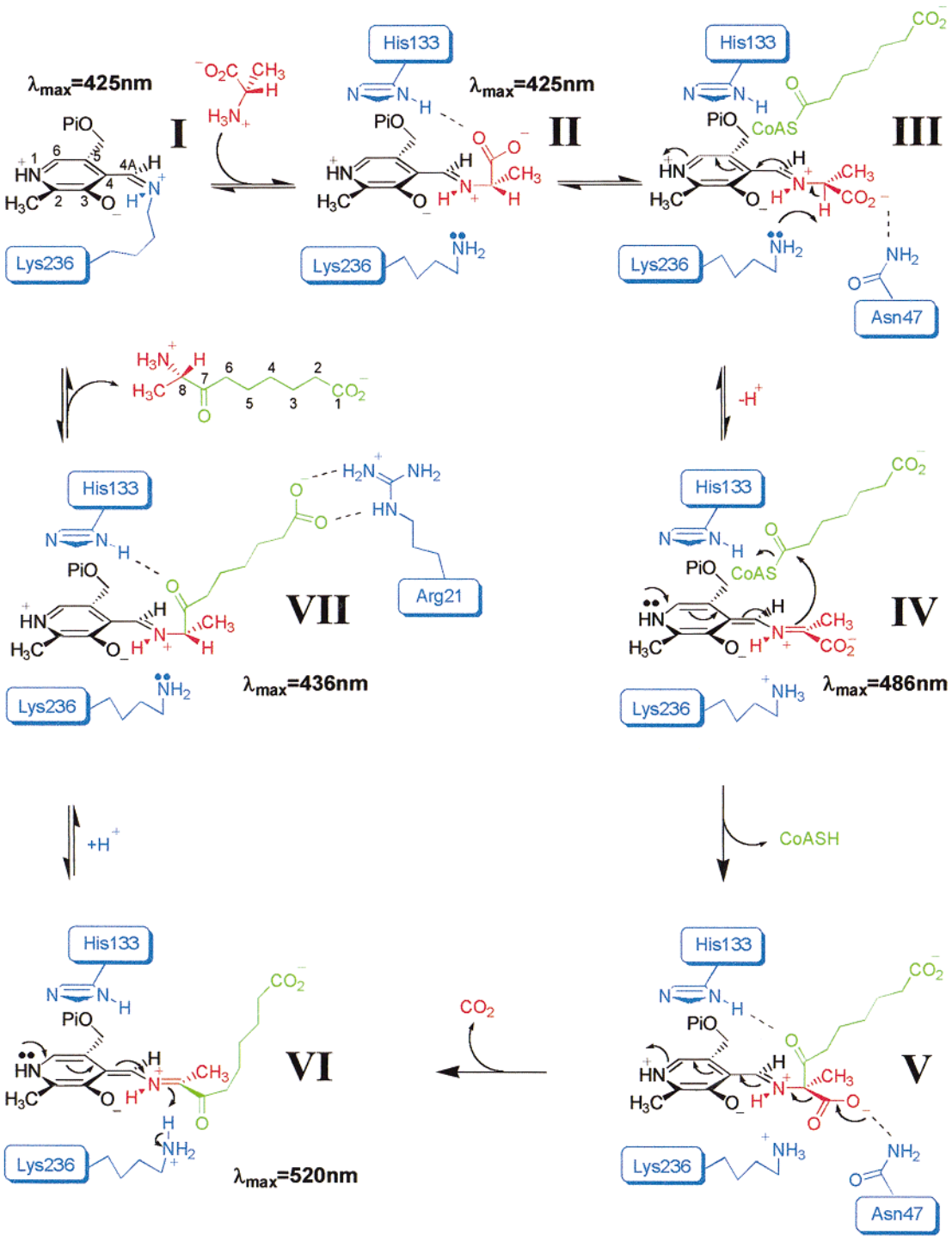

FIGURE 3: Proposed reaction mechanism for AONS. The atoms of L-alanine are red, the atoms of pimeloyl-CoA green, the amino acids of the enzyme blue, and the PLP cofactor black. Roman numerals represent intermediate transition states.

in the dissociation constant (K_d = 4.5 mM). These results are in broad agreement with those obtained for the corresponding *B. sphaericus* enzyme which exhibits decreases in the L- and D-alanine dissociation constants in the presence of pimeloyl-CoA (*27*).

Pre-Steady-State Kinetics. The increase in the external aldimine absorbance at 425 nm upon addition of L- or D-alanine was exploited to determine the pre-steady-state rate constants for external aldimine formation (Figure 5). The second-order rate constant for L-alanine is 2×10^4 M^{-1} s^{-1}, while D-alanine forms an external aldimine more than 100 times slower with a rate constant of 125 M^{-1} s^{-1}.

The formation of the substrate quinonoid intermediate (Figure 3, IV) was studied by measuring absorbance changes at 486 nm. The kinetics of quinonoid formation are complex (Figure 6). Instead of an expected immediate monophasic single-exponential increase corresponding to quinonoid formation, a lag of ~30 ms is observed. This lag appears to be independent of temperature (10−30 °C). This is followed by a sharp increase in absorption with a single-exponential rate of 45 s^{-1}. A third, slow phase (corresponding to formation of intermediate and product complexes) follows, which fits to a single exponential with a rate of 2.8 s^{-1}. The exact rate constants for each process could not be determined

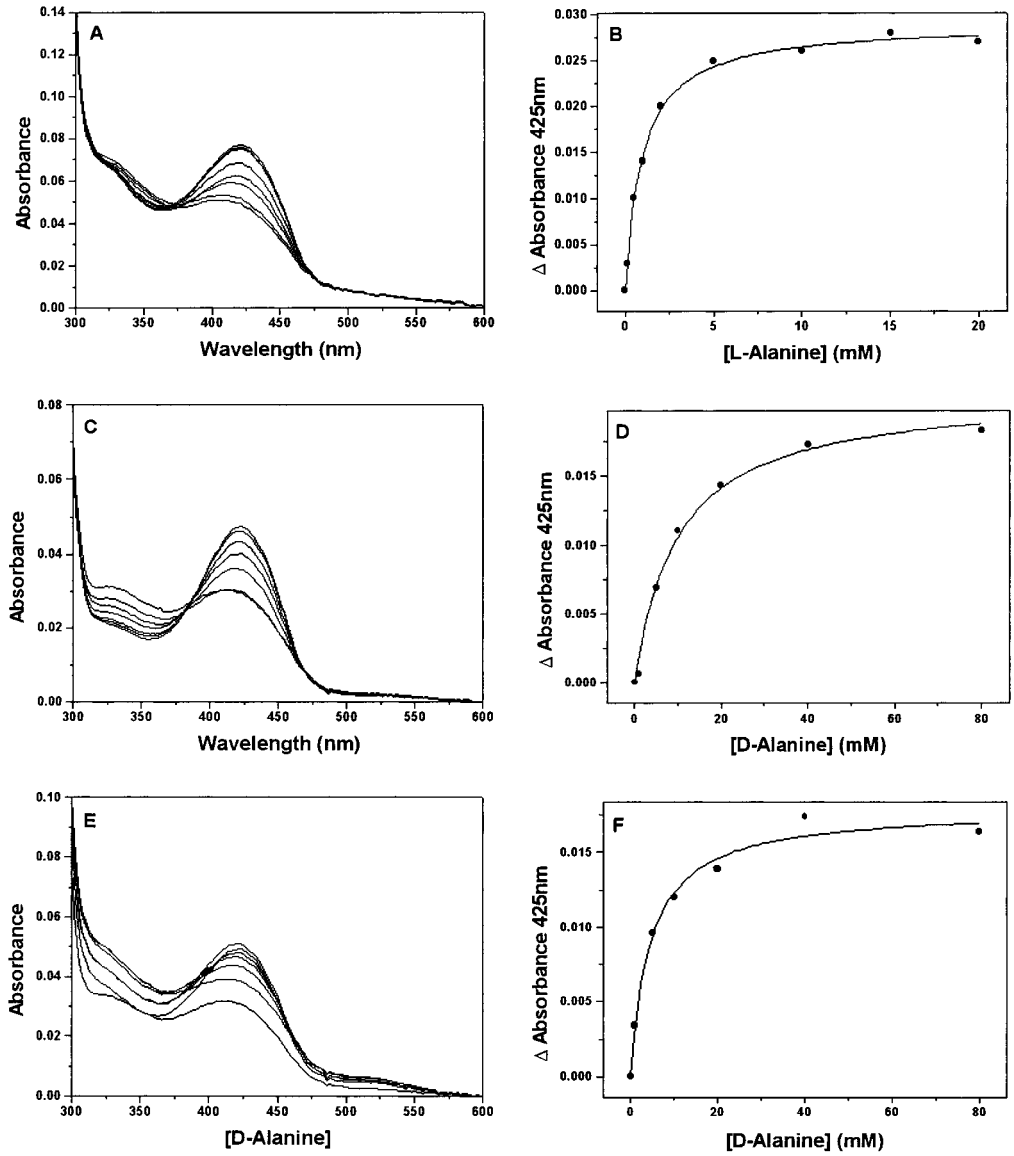

FIGURE 4: Binding of L- and D-alanine to AONS. The enzyme was equilibrated with L- or D-alanine in the presence or absence of pimeloyl-CoA. The increase in absorbance was plotted vs the titrant concentration. Data were fitted to a hyperbolic saturation curve (eq 1): (A) 25 μM AONS equilibrated with L-alanine (from bottom to top, 0, 0.1, 0.5, 1, 2, 5, 10, 15, and 20 mM) in the absence of pimeloyl-CoA, (B) $K_d = 0.9 \pm 0.1$ mM, (C) 25 μM AONS equilibrated with D-alanine (from bottom to top, 0, 1, 5, 10, 20, 40, and 80 mM) in the absence of pimeloyl-CoA, (D) $K_d = 9.8 \pm 1.4$ mM, (E) 25 μM AONS equilibrated with D-alanine (from bottom to top, 0, 1, 5, 10, 20, 40, and 80 mM) in the presence of 143 μM pimeloyl-CoA, and (F) $K_d = 4.5 \pm 0.7$ mM.

accurately due to the small absorbance changes at low pimeloyl-CoA concentrations.

Structure of the Holoenzyme. We have previously reported and analyzed the X-ray structure of the enzyme in complex with the PLP cofactor at a resolution of 1.9 Å (*6*). We have since been able to collect better data (Table 3) and refined the structure in the resolution range from 10 to 1.67 Å (43 791 unique reflections) to a final *R* factor of 18.6% using SHELX97. The rms deviation from ideality for the bond lengths was 0.009 Å and for the valent angles, 2.3°. The final model contained 384 amino acids (mean $B = 31.3$ Å^2), 232 fully occupied water molecules (mean $B = 38.0$ Å^2), 254 partially occupied water molecules (occ = 0.5, mean $B = 38.0$ Å^2), and three phosphate ions. The atoms of PLP had a mean temperature factor of 30.6 Å^2. This refined model has revealed more details of the active site.

The PLP−Lys236 Complex Is Distorted. The torsion angle around the single C4−C4A bond of the pyridoxal cofactor defines whether the double bond between the NZ of the Lys236 and the C4A of the PLP is coplanar with the pyridoxal ring. In the planar configuration, the electrons of the double bond are conjugated with the delocalized electrons of the pyridine ring (indicated by the band at 425 nm in the absorption spectrum, Figure 2A). The band observed at 334 nm can be attributed to a non-coplanar arrangement. The presence of the 425 nm band in our PLP−enzyme spectra suggests that the C4A═NZ double bond is coplanar with the aromatic ring of PLP and the C3−C4−C4A═NZ torsion angle is close to 0°. In the crystal structure, however, this angle is 54° which is far from coplanarity and apparently inconsistent with our spectroscopic results. The pyridine ring and the atoms attached to the NZ═C4A double bond were separately constrained to idealized planar geometry during the refinement, but the shape of the electron density around the cofactor suggests that the imposed restraints drive C4A of PLP out of the center of the electron density, although

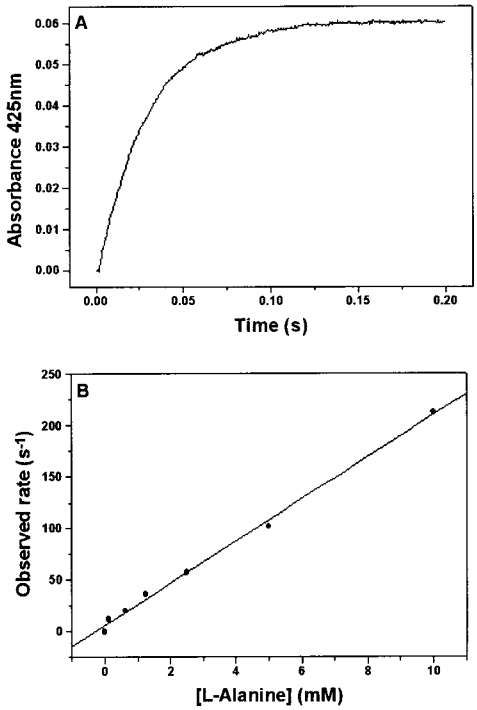

FIGURE 5: Pre-steady-state kinetics of external aldimine formation. (A) Stopped-flow trace of 20 μM AONS mixed with 10 mM L-alanine. The formation of external aldimine was monitored at 425 nm. (B) Plot of observed rate vs L-alanine concentration. Data were fitted to a linear regression, the gradient of which gave a rate k_1 of $(2 \pm 0.6) \times 10^4$ M^{-1} s^{-1}. A plot of the data for the reaction with D-alanine gave a rate k_1 of 125 ± 0.01 M^{-1} s^{-1}.

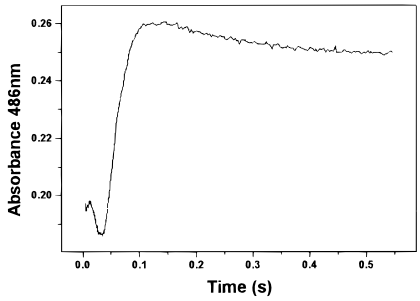

FIGURE 6: Pre-steady-state kinetics of quinonoid formation. AONS (25 μM) pre-equilibrated with 10 mM L-alanine mixed with 210 μM pimeloyl-CoA. The appearance of the quinonoid band was monitored at 486 nm.

the resolution of 1.7 Å is too low to be absolutely definitive. Compared to those of the neighboring covalently linked atoms, the temperature factors of the double-bonded C4A and NZ are 8 Å^2 greater. The C4A atom is about 0.3 Å out of plane from the PLP ring, against the imposed planarity restraints. The C4A=NZ double bond remains undistorted and flat, and the C4A=NZ−CE bond angle is 130° and close to the accepted ideal value of 132°. The major distortions from the ideal geometry are associated with the C4−C4A= NZ bond angle of 108° which is far from the target value of 122°.

Glu175 Is Negatively Charged. The carboxylate of Glu175 is hydrogen-bonded to the main chain amides of His133 and Ser179 and to the hydroxyl of Ser179. The electron density map shows that the Glu175 carboxylate does not make any other direct contacts with the other protein atoms or water molecules. This environment of the Glu175 carboxylate suggests that it has developed a negative charge which can polarize the hydroxyl of Ser179.

Pyridoxal−Enzyme Interactions. The aromatic ring of PLP is sandwiched between the hydrophobic side chains of Ala206 and Thr233 on one side (not shown) and His133 on the other (Figure 7A). The carboxylate of Asp204 is hydrogen-bonded to N1 of PLP, and C4A is covalently bound to the NZ of Lys236. The O3 is hydrogen bonded to His207. If the nitrogen ND1 of His207 is protonated, then this proton is coplanar with the pyridoxal ring. The other nitrogen of His207 (NE1) is hydrogen bonded to the hydroxyl of Tyr49 which is coordinated to Asn47 and Arg361 through a water molecule (Figure 7A). This water molecule is perfectly coordinated in the center of a triangle formed by the NH1 of Arg361, the hydroxyl of Tyr49, and the amide oxygen of Asn47. The ND and NH1 of Arg361 are hydrogen bonded to the main chain carbonyls of Met180 and Ser179 which is coordinated to Glu175. This interconnecting network of hydrogen bonds is rearranged during catalysis (Figures 7B and 9).

Structure of the AON−PLP−Enzyme Complex. The structure of AONS incubated with its product, AON, was determined to 2.0 Å resolution in space group $P3_112$. The unit cell parameters of the soaked crystals remain close to those of the holo form of the enzyme (shown in parentheses) [$a = b = 58.9$ (58.7) Å, $c = 200.8$ (200.2) Å] but are significantly different from those of the apo form (*6*). The R factor between the observed structure factor amplitudes of the AON-soaked ($F_{aon-plp}$) and of the holoenzyme crystals (F_{plp}) is 29.7%. The difference map calculated with coefficients $F_{aon-plp} - F_{plp}$ and $PHI_{plp-calc}$ shows unambiguously that AON is bound, but the connectivity of the difference electron density for the ligand is poor. We performed rigid-body refinement of the AON-free model (without water molecules and PLP) with the AON-bound data. The difference map calculated with coefficients $F_{aon-plp} - F_{calc}$ and PHI_{calc}, where calc refers to the rigid-body-refined AON-free model, clearly shows the connected electron density for the PLP−AON complex at the 2.5σ level. The electron density of the enzyme was very poor in the region between residues 320 and 361. The model of AON−PLP was fitted into the difference density map; the region between residues 320 and 361 was rebuilt and the structure refined with SHELX97 in the resolution range of 10−2.0 Å (27 177 unique reflections) to a final R of 21.2% ($R_{free} = 26.4\%$). The mean temperature factor for the AON atoms in the final refined model is 36.1 Å^2, about the same as for all protein atoms (36.8 Å^2) and 6 Å^2 greater than that for the atoms of PLP (30.9 Å^2). The solvent model had 170 fully occupied water molecules (mean $B = 37.5$ Å^2), 175 partial water molecules (occ = 0.5, mean $B = 29.5$ Å^2), and three phosphate ions. The rms deviation from ideality for the bond lengths was 0.007 Å and for the valent angles 2.1°. The geometry of the pyridoxal ring in the AON−PLP complex is undistorted compared to that of the holoenzyme. The electron density around the AON−PLP complex is shown (Figure 8).

C-Terminal Domain Movement. The overall refined protein structure of the complex is close to that of the holoenzyme, and the rms deviation between all Cα atoms is 1.2 Å after superposition (Figure 7C). The enzyme molecule moves about 0.3 Å as a whole approximately along the crystal-

Table 3: Details of Data Collection and Refinement[a]

	resolution (Å)	completeness (%)	1/sigI	R_{merge} (%)	multiplicity	unit cell *a*	unit cell *c*	*R* (%)	R_{free} (%)
holo form	1.67	100.0 (99.9)	16.7 (1.6)	8.0 (60.8)	4.9 (5.2)	58.87	200.80	18.6	24.5
AON	1.99	96.5 (93.5)	6.3 (1.3)	6.5 (45.2)	2.9 (2.7)	58.89 (+0.02)	201.77 (+1.03)	21.23	27.8

[a] The numbers in parentheses refer to the outer resolution shell. Both data sets were collected at 100 K. The data from the holoenzyme crystals were collected at beamline X11 (EMBL/DESY) at a wavelength of 1.0 Å. The data from the crystals of the product−enzyme complex were collected at station 7.2 (SRS, CLRC Daresbury Laboratory, Warrington, U.K.) at a wavelength of 1.488 Å.

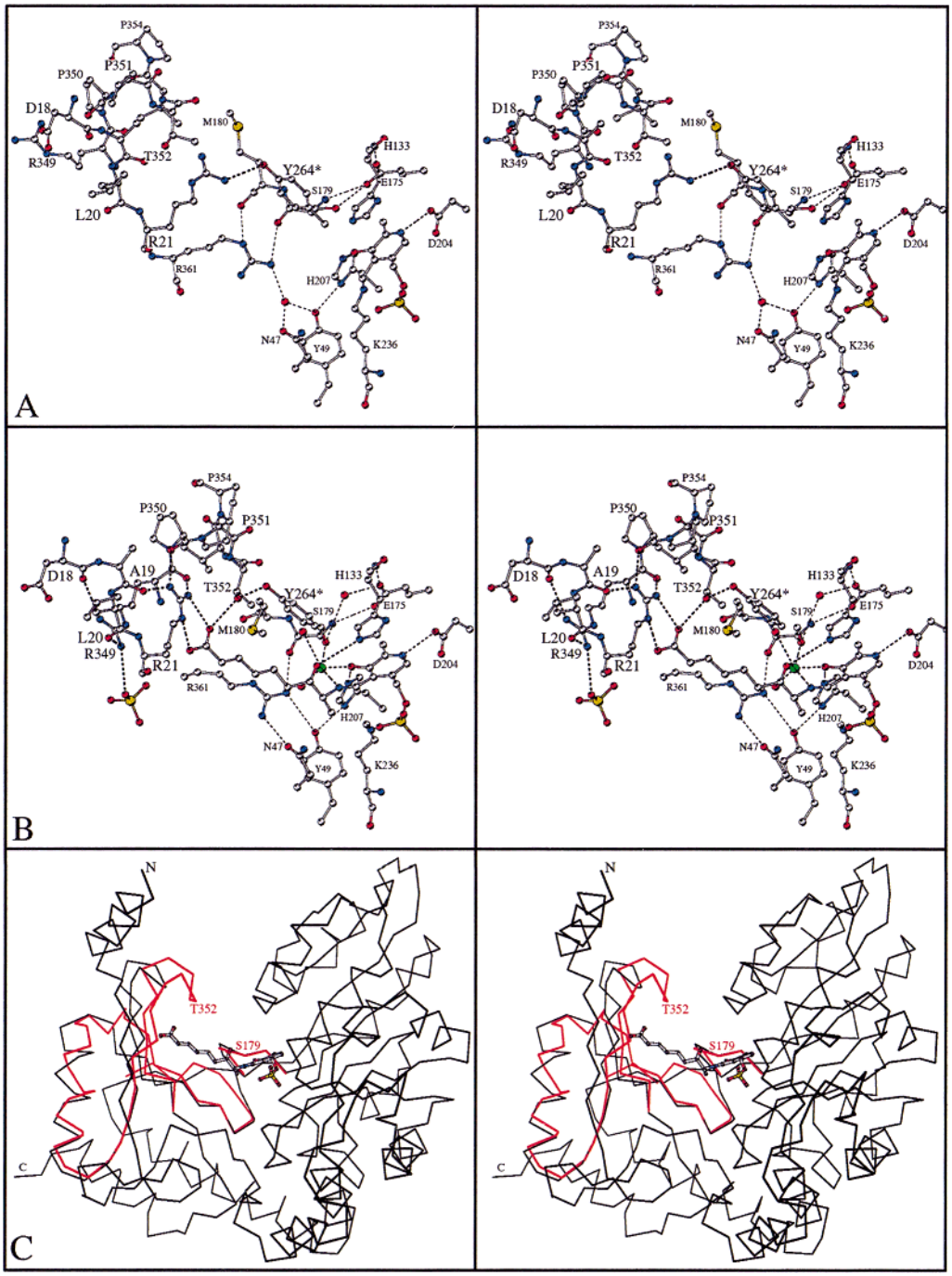

FIGURE 7: X-ray structures of AONS. The stereoimages illustrate the conformational transitions upon product binding to the holoenzyme. Panels A and B show in detail how the structure of the holoenzyme (upper stereopair) accommodates AON (lower stereopair). Panel C shows the overall movement of the C-terminal domain (in red) upon AON binding as an overlay of the Cα atoms. The bulk of the structure remains unaltered. In all three panels, the view is through the omitted monomer of the dimeric enzyme toward the AON−PLP binding site. An asterisk indicates residues from the omitted monomer.

lographic dyad axis. This movement preserves the mutual orientation of the monomers within the crystallographic homodimer. The β-sheet of the C-terminal domain undergoes a conformational transition, but the rest of the enzyme backbone remains practically unchanged; the rms deviation between Cα atoms for the first 320 amino acids is only 0.3

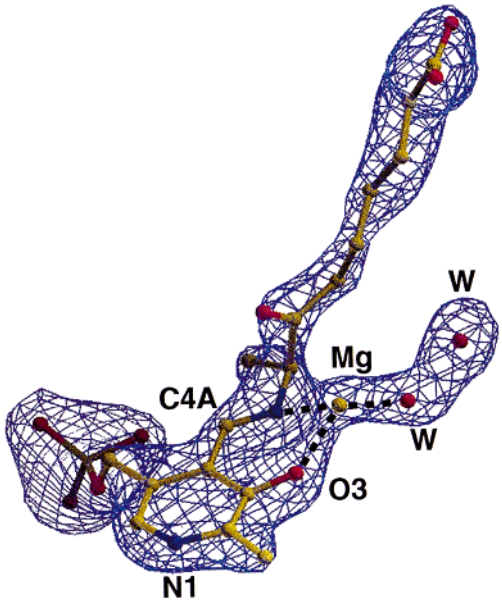

FIGURE 8: Electron density map for the AON external aldimine. The sigmaA-weighted $(2F_{obs} - F_{calc})PHI_{calc}$ as calculated by SHELX97 and contoured at the 1.8σ level.

Å (Figure 7C). For the next 40 amino acids of the C-terminal domain, it rises to 2.1 Å. Three β-strands (colored red in Figure 7C) of the flexible domain fold toward the active site of the AONS catalytic dimer (*6*). The Cα of Thr352 is at the tip of the flexible domain and moves 5.5 Å toward the main domain, narrowing the path of access to the active center. The conformational transition involves unwinding the last turn of the helix (colored red in Figure 7C). Residues 324−334 that connect the moving domain and this helix are in a region of poor electron density, are disordered, and have very high temperature factors.

AON−PLP Aldimine Complex. The C8 atom of the bound AON is clearly tetrahedral, and the C8(AON)−N8(AON)−C4A(PLP)−C4(PLP) dihedral angle is close to 180°. This implies that N8 and C4A, rather than C8 and N8, are connected by the double bond and shows that the PLP−AON complex is an external aldimine and not a quinonoid form. The N8═C4A double bond is coplanar with the pyridine ring, and the AON−PLP complex does not exhibit any significant deviations from idealized geometry.

Mg^{2+} Ion. The negatively charged carboxylate of Glu175 and the hydroxyl of Ser179, which were hydrogen bonded in the holoenzyme structure, move apart in the AON-bound structure (Figure 9). This makes room for a water molecule to be bound between them (Figure 9B). A further electron density peak is found between O3 and N8 close to the plane of the pyridoxal ring of the AON−PLP complex (Figure 8). There were no model atoms in the close vicinity of the peak until the last stages of the refinement, and so it cannot be attributed to the model bias. The peak is at 2.1 Å from both O3 and N8 and by geometry is consistent with a Mg^{2+} ion rather than with a water molecule. The ion is closely coordinated to five atoms: the oxygen O3, the hydroxyl of Ser179, the nitrogen N8, and two water molecules. The occupancy of Mg^{2+} refines to a value of 0.9 if we fix its temperature factor at the average value for the AON atoms (36.1 $Å^2$).

Conformational Changes in the PLP Binding Site. The coordination of the PLP phosphate group to the enzyme remains practically the same as in the holoenzyme (*6*). Compared to the orientation in the holoenzyme, the pyridine ring of the AON−PLP complex is rotated about 15° around the C5−C5A bond such that the O3 and C4A atoms move away from the catalytic Lys236 (panels A and B of Figure 7). The rotation of the PLP ring is accompanied by a similar rotation of His133 which remains stacked above the PLP ring and follows its movement. The NZ of Lys236 now binds to the phosphate of PLP. This conformation is similar to the orientation of Lys236 in the apo form of the enzyme, where the phosphate of PLP is mimicked by a free phosphate from the crystallization medium (*6*). Another important feature of the complex is the hydrogen bond between the O7 of AON and His133.

In the holoenzyme structure, NE2 of His207 is hydrogen bonded to O3 of the PLP ring at a distance of 2.5 Å. His207 tracks the movement of O3, allowing its NE2 to remain bound to O3 of PLP. This distance remains unchanged between the holoenzyme and the product aldimine forms.

The hydroxyl of the Ser179 turns toward O3 of PLP in the AON-bound structure (Figure 9). The rotation of the Ser179 side chain is accompanied by a small movement of the Val177−Asp185 loop which brings the Ser179 side chain 0.6 Å closer to O3 (Figure 7A−C). The ND1 and NH1 of Arg361, which are hydrogen bonded to the main chain carbonyl oxygens of Ser179 and Met180 in the holoenzyme, move toward Tyr49 and Asn47 and eliminate the water molecule which was coordinated to Asn47 and Tyr49. NH1 and NH2 of Arg361 in the AON-bound enzyme now coordinate to Tyr49 and Asn47 side chains directly (Figure 7B). The hydroxyl of Tyr49 is hydrogen bonded to the ND1 of His207 in both forms of the enzyme.

Hydrophobic Interactions in the AON−PLP Complex. The methylene chain of AON is in van der Waals contact with the Val79 side chain and is aligned along the plane of Tyr264* (the asterisk signifies a residue from the opposite monomer of the dimeric enzyme). The opposite monomer has one more hydrophobic side chain (Ile263*) interacting with the ligand (not shown). In the holoenzyme, Tyr264* and Ile263* face a water-filled channel between the monomers. A significant feature of AON binding is the rotation of the Met180 side chain toward the AON and away from Leu131. Leu131 now establishes a hydrophobic contact with Pro350 which moves toward it as a result of the conformational transition of the C-terminal domain.

Binding of the AON−PLP Carboxylate. The carboxylate of AON is bound to Arg21 from the N-terminal domain and Arg349 from the C-terminal domain. In the holoenzyme, Arg21 is hydrogen bonded to Tyr264* and Arg349 is hydrogen-bonded to the Asp18 of the N-terminal domain. The conformational transition of the C-terminal domain brings these arginines close together so that they align antiparallel to each other and establish the new relative positions of the C- and N-terminal domains. In the AON-bound enzyme, Arg21 connects the main chain carbonyl oxygens of Ala19, Pro350, and Arg349 with the carboxylate tail of AON. The side chain of Arg349, which is hydrogen bonded to the carboxylate of Asp18 in the holoenzyme, moves together with the C-terminal domain of the AON-bound form and now binds to the main chain carbonyls of Leu20 and Asp18 of the N-terminal domain. These two arginine "arms" stretch from the opposite N- and C-terminal

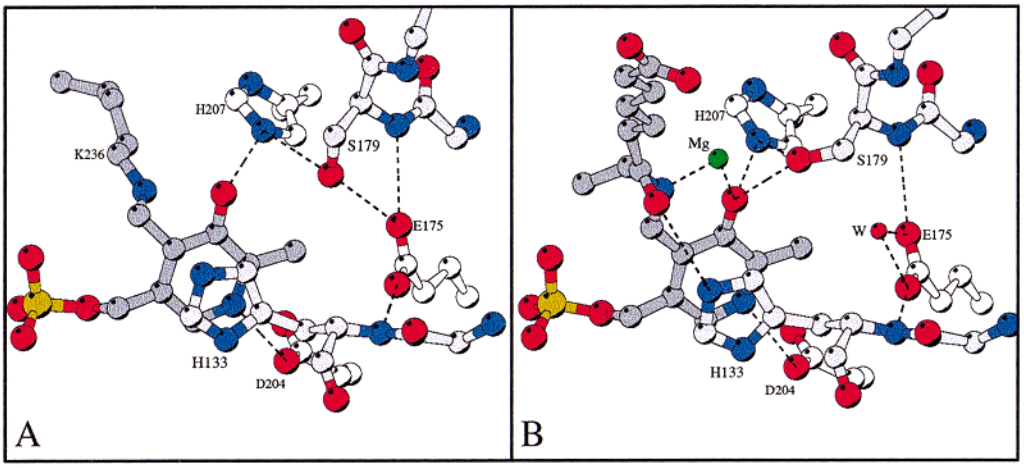

FIGURE 9: Cofactor binding site. The key residues in the structures of the PLP internal aldimine (A) and the AON−PLP external aldimine (B) are shown. The carbons of the PLP complexes in both pictures are dark gray, and His133 above the pyridine ring is gray.

domains binding them together. The Tyr264* that is bound to the Arg21 in the holo structure is coordinated to the hydroxyl of Thr352 which in turn is hydrogen bonded to the carboxylate of AON in the AON-bound form.

Phosphate Binding Sites. A new phosphate binding site is created in the AON-bound enzyme. The electron density for the phosphate is clear, but the temperature factors are high. When all of the phosphate atoms were assigned an average temperature factor of 37 Å^2, the occupancy refined to 0.6. The phosphate (Figure 7B) is coordinated to the Arg349 and to water molecules (not shown). Another phosphate (not shown), which we located in the arginine-rich region and tentatively proposed as the CoA binding site, is absent in the structure of the AON-bound form (*6*).

DISCUSSION

We have combined our results to build a consistent model of the AONS reaction mechanism which is discussed in terms of the individual steps of the reaction as summarized in Figure 3.

(I) The Internal Aldimine Is Flexible. The conventional explanation of the two absorption bands exhibited by PLP internal aldimines is that the 425 and 334 nm bands represent protonated and unprotonated forms of the imine nitrogen (*28*). In the crystal structure of the AONS holo form (and in many other PLP enzymes), the C4A=NZ double bond is not coplanar with the pyridine ring. The fact that in AONS the absorption spectra do not exhibit any significant pH dependence (between pH 6.0 and 8.5) suggests that the problem may be more complex. The lower-wavelength band may correspond to a non-coplanar state (which may be protonated or unprotonated). The transition between the nonplanar and planar forms of the internal aldimine can easily be accommodated by the enzyme active site without any major conformational changes as has been shown for mitochondrial aspartate aminotransferase (*29*). It is plausible that crystallization selects the nonplanar form or that the structure comprises a mixture of two species, and we are not able to detect the minor coplanar component at our resolution of 2.0 Å.

The pH dependence of aspartate aminotransferase and tryptophanase spectra has been attributed to a reduction in the pK_a of the Schiff's base nitrogen, caused by interaction with an acidic amino acid (Asp204 in AONS) which increases the pK_a of the N1 of pyridine (*13*, *30*). Protonation of NZ in the pH-dependent enzymes promotes the O3−NZ hydrogen bond and shifts the equilibrium toward the planar conformation absorbing at 425 nm. In our case, the pH independence of the AONS spectra indicates that the pK_a of NZ in AONS is much higher than in aspartate aminotransferase and tryptophanase. Thus, the imine nitrogen is always protonated, implying that the equilibrium between the two spectral forms may be defined by the conformational flexibility of the internal aldimine within the active site. The presence of two conserved amino acids (Glu175 and Ser179) which interact with O3 of the pyridine ring (Figures 7A and 9A) may enhance the influence of Asp204 on the pK_a of the imine nitrogen.

It is generally accepted that external aldimine formation proceeds via a transient geminal diamine intermediate where the nitrogen NZ of the catalytic lysine and the nitrogen of alanine lie on opposite sides of the pyridine plane (*31*). The imine nitrogen must be protonated for formation of this intermediate, and a small rotation around C4−C4A places the NZ close to the position it has to adopt in the symmetrical diamine intermediate. The negatively charged O3 is free and may accept a proton from the amino group of the incoming L-alanine. We suggest that this conformation, rather than the planar one, may be the reactive species.

The pH-dependent mechanisms of aspartate aminotransferase and tryptophanase imply that the substrate amino group proton is abstracted by O3 of the pyridine and transferred to NZ prior to geminal diamine formation. In AONS, the proton of the substrate amino group could be abstracted in an analogous manner, but in this case, the necessary removal of the proton from O3 involves the His207-Ser179-Glu175 system previously described (Figures 7 and 9). The comparison of the crystal structures of the apoenzyme, the holoenzyme, and the AON−PLP complex shows that the Ser179 hydroxyl can swing between O3 and Glu175, and this may be essential for catalysis.

(II) Substrate External Aldimine. L-Alanine forms an external aldimine complex ($k_1 = 2 \times 10^4$ M^{-1} s^{-1}) with AONS. If the mechanism of AONS is sequential ordered, we would expect k_1 to approximate k_{cat}/K_m for L-alanine. The fact that k_{cat}/K_m is less than k_1 for L-alanine suggests that

there may be a slow step following external aldimine formation that is necessary for productive binding of pimeloyl-CoA. D-Alanine is not a substrate for AONS, but it is also able to form an external aldimine complex, albeit about 160 times slower than L-alanine. Modeling of the D-alanine external aldimine orientates the methyl group of D-alanine toward O3 and the Ser179-Glu175 pair. This unfavorable contact may explain the slower kinetic constant for external aldimine formation.

Equilibrium binding studies indicate that external aldimine (II) formation for D-alanine is enhanced by the presence of the second substrate, pimeloyl-CoA. We speculate that the dissociation constant for D-alanine is reduced by binding of pimeloyl-CoA which blocks its exit path from the bottom of the binding site. It is also conceivable that pimeloyl-CoA induces a conformational change which leads to a more tightly bound external aldimine species.

An absorption peak at a longer wavelength, which is associated with quinonoid formation, is not observed for either L- or D-alanine. It seems that binding of L-alanine alone is insufficient to promote noticeable proton abstraction at Cα. A study of *B. sphaericus* AONS shows that exchange of the Cα proton does occur, but is slow (*16*). We were unable to crystallize the L-alanine external aldimine complex but have modeled it by analogy with our product external aldimine structure. If we assume that the alanine−PLP aldimine adopts a conformation similar to the AON−PLP complex, then one of the carboxylate oxygens of the alanine−PLP aldimine will take the position of the C7 carbonyl which in the product is hydrogen bonded to the His133 ring. This configuration places the Cα hydrogen of alanine away from the catalytic Lys236, making it unavailable for abstraction. Instead, the methyl group points toward Lys236 and blocks its access to the Cα position. Proton abstraction requires a rotation around the N−Cα bond in the pyridine plane which directs the Cα proton toward Lys236. This orientation of the complex places the Cα carboxylate within hydrogen bonding distance of the side chain of Asn47.

Quinonoid formation is enabled by the addition of the second substrate, pimeloyl-CoA (k_{obs} = 45 s^{-1}). This is preceded by a ∼30 ms lag phase which we attribute to conformational transitions of both the enzyme and the alanine−PLP external aldimine. We suggest that when pimeloyl-CoA docks in the active site its thioester carbonyl binds to His133, displacing the carboxylate oxygen of alanine from His133. Rotation around the N−Cα bond of the alanine−PLP aldimine places the Cα proton in a position perpendicular to the pyridine ring facing Lys236 in accordance with the Dunathan hypothesis (*32*). The proximity of Lys236 to Cα leads to rapid abstraction of the proton and creation of a resonance-stabilized quinonoid intermediate as indicated by the band at 486 nm.

(III) Conformational Transition of the Enzyme. The conformation observed in the product complex indicates that the position of the flexible C-terminal domain is stabilized by the pimelate carboxylate, which acts as an important interdomain linker. It is reasonable to assume that the binding patterns of the pimelate chain of pimeloyl-CoA and AON−PLP are similar and that a conformational transition does in fact take place following pimeloyl-CoA binding. This is consistent with the lag phase observed prior to quinonoid formation. Movement of the C-terminal domain in the AON−PLP structure brings Arg361 closer to the putative position of the alanine carboxylate. The proximity of this positive charge may help to polarize the external aldimine (II), facilitating proton abstraction by Lys236.

Following deprotonation at Cα of the alanine external aldimine, our modeling suggests that the positively charged amino group of Lys236 moves toward the phosphate of PLP while the carboxylate of alanine remains coordinated to Asn47. This model is corroborated by the position of the Lys236 side chain in the apoenzyme and product structures. At present, we do not have any structural information about the binding of the CoA moiety. However, the positions of the free phosphates arising from the crystallization medium may indicate the binding sites of the CoA phosphates (*6*).

(IV) Condensation with Pimeloyl-CoA. Modeling of the first quinonoid intermediate (IV) suggests that one of the oxygens of the alanine carboxylate is coordinated to the amide of Asn47. The other carboxylate oxygen occupies the position of the Mg^{2+}-coordinated water molecule, which is coplanar with the pyridine ring in the AON-bound structure (Figure 7B). While it is tempting to suggest that a Mg^{2+} ion might somehow be involved in the quinonoid structure at this stage, we found that the enzymatic activity is not Mg^{2+}-dependent, suggesting that active involvement of the Mg^{2+} ion in catalysis is unlikely and that this position is occupied instead by the imine proton.

Following the pimeloyl-CoA-induced Cα deprotonation, the quinonoid attacks the thioester carbonyl of pimeloyl-CoA, liberating HSCoA and producing a β-ketoacid−aldimine complex.

(V) Decarboxylation. The only difference between the β-ketoacid intermediate (V) and the product−PLP complex (VII) is the presence of the carboxylate group instead of the Cα proton. It is reasonable to assume that both complexes adopt similar conformations. The pyridine oxygen O3, the hydroxyl of Ser179, and the carboxylate of alanine create a local negative charge which is even greater than that in the product−PLP complex (VII) where, in the crystal, a Mg^{2+} ion is coordinated.

At present, the mechanism of decarboxylation is unknown. However, it could conceivably proceed by one of three distinct routes: (a) a mechanism, similar to that found in most PLP-dependent decarboxylases, in which the pyridine ring acts as the electron sink (*32*); (b) formation of a protonated C7 imine as an electron sink in a process similar to the mechanism of 3-oxybutyrate decarboxylase (*33*); or (c) a route in which the C7 ketone could be protonated by the adjacent His133 to form an electron sink.

While it is not possible, on the basis of current experimental evidence, to eliminate any of these possibilities, our modeling of the intermediate (V) and the fact that enolization of the C7 ketone occurs and that the product external aldimine is in equilibrium with its quininoid form (vide infra) suggest that route (c) has to be considered as a likely candidate (*16*).

(VI) Quinonoid Intermediate Formation Requires a Conformational Change. As described above, the formation of a planar quinonoid intermediate (VI) requires a rotation of about 90° around the C8−N8 bond. If it is assumed that the position of the pimelate carboxylate remains constant throughout the enzyme reaction, this transition has to involve

a significant rotation of the pyridine ring to allow the pimelate carboxylate to reach its binding site. The planarity of the quinonoid (VI) is corroborated by the presence of the long-wavelength band at 520 nm in the spectrum of the product−PLP aldimine complex. Previous studies have demonstrated that the C6 pimelate proton can be slowly exchanged following the formation of the quinonoid (VI) (*16*). The flat geometry of the quinonoid (VI) brings C6 closer to Lys236 and may be the explanation for this exchange.

(VII) Product−PLP External Aldimine. The enzyme is capable of forming a stable external aldimine complex with the product of the reaction. Soaking crystals with AON at high concentrations allowed us to determine the crystal structure of the product−PLP external aldimine complex. Although there is an equilibrium between this species and the quinonoid (VI) in solution, we can see no indication of this in the crystal structure.

The observed conformation of the product-bound form of the enzyme, in comparison with the holoenzyme structure, shows a major movement of the C-terminal domain which closes the path of access to the binding site (Figure 7). Because this "closed" conformation of the enzyme-bound product external aldimine is stabilized by the interactions around the pimelate moiety, we suggest that the transition is the result of a major conformational change in the protein which is caused by pimeloyl-CoA binding prior to this step in the reaction sequence. In the product external aldimine, the hydrophobic chain of the pimelate (from C2 to C6) is completely surrounded by hydrophobic enzyme residues. The deep binding pocket of the holoenzyme is wide enough to accommodate pimeloyl-CoA in its free configuration, and binding to the enzyme separates the two hydrophobic patches (i.e., the pantothenate and pimeloyl chains) of pimeloyl-CoA. The C-terminal domain of the enzyme closes over the pimelate chain, leaving the pantothenate arm to stick out from the binding pocket.

The conformation of the external aldimine (VII) is stabilized by a Mg^{2+} ion. It is likely that this ion arises from the solution of synthetic AON which we used for soaking experiments (there were no magnesium salts in the crystallization mixture). Our search of the Cambridge small molecule structural database revealed that the structures of most pyridoxal aldimines are flat and contain a metal ion (usually Cu^{2+}, Ni^{2+}, or Co^{3+}) in a position analagous to that of our Mg^{2+} ion, which chelates to O3 and N8. The enzymatic reaction does not depend on the presence of Mg^{2+} or monovalent ions, though Mg^{2+} is obviously able to substitute for the proton of N8 in the crystal structure of the product aldimine (VII). The protonation of the quinonoid (VI) leaves the amino group of Lys236 deprotonated and capable of rapid Schiff base formation. In our crystal soaking experiment, we artificially reversed the final transimination reaction using a high concentration of the product to form the AON external aldimine, and the binding of a Mg^{2+} ion could be inferred to be an artifact.

The final stage of the reaction sequence leading to product release and reformation of the internal aldimine requires transimination of the product aldimine by Lys236 and reversal of the induced conformational changes in the C-terminal protein geometry. These processes may conceivably be rate-limiting steps in the catalytic mechanism.

Conclusion. These results point to a mechanistically reasonable pathway for the catalytic action of AONS which may prove to be common to other members of the physiologically important α-oxoamine family of enzymes. However, consolidation of these results awaits detailed analysis of the role of active site residues and the explanation of the involvement of the conformational changes in the protein during catalysis.

ACKNOWLEDGMENT

We are grateful to BBSRC for providing access to the synchrotron radiation source at CCLRC Daresbury Laboratory and to EMBL/DESY for the opportunity to collect data at beamline X11. Thanks are also due to Drs. A. Munro and M. Noble for help with the analysis of the pre-steady state kinetic data, to Dr. E. Chrystal (Zeneca) for helpful discussions, and to Ms. L. J. Mullan, Ms. M. I. Brunton, and Ms. L. McIver for technical assistance.

REFERENCES

1. Eisenberg, M. (1987) *Biosynthesis of biotin and lipoic acid*, Vol. 1, American Society for Microbiology, Washington, DC.
2. Alexander, F. W., Sandmeier, E., Mehta, P. K., and Christen, P. (1994) *Eur. J. Biochem. 219*, 953−960.
3. Mehta, P. K., and Christen, P. (1994) *Biochem. Biophys. Res. Commun. 198*, 138−143.
4. Grishin, N. V., Phillips, M. A., and Goldsmith, E. J. (1995) *Protein Sci. 4*, 1291−1304.
5. Toney, M. D., Hohenester, E., Cowan, S. W., and Jansonius, J. N. (1993) *Science 261*, 756−759.
6. Alexeev, D., Alexeeva, M., Baxter, R. L., Campopiano, D. J., Webster, S. P., and Sawyer, L. (1998) *J. Mol. Biol. 284*, 401−419.
7. John, R. A. (1995) *Biochim. Biophys. Acta 1248*, 81−96.
8. Inoue, Y., Kuramitsu, S., Inoue, K., Kagamiyama, H., Hiromi, K., Tanase, S., and Morino, Y. (1989) *J. Biol. Chem. 264*, 9673−9681.
9. Toney, M. D., and Kirsch, J. F. (1993) *Biochemistry 32*, 1471−1479.
10. Yoshimura, T., Bhatia, M. B., Manning, J. M., Ringe, D., and Soda, K. (1992) *Biochemistry 31*, 11748−11754.
11. Lu, Z., Nagata, S., McPhie, P., and Miles, E. W. (1993) *J. Biol. Chem. 268*, 8727−8734.
12. June, D. S., Suelter, C. H., and Dye, J. L. (1981) *Biochemistry 20*, 2714−2719.
13. Jhee, K.-H., Yang, L., Ahmed, S. H., McPhie, P., Rowlett, R., and Miles, E. W. (1998) *J. Biol. Chem. 273*, 11417−11422.
14. Laber, B., Gerbling, K.-P., Harde, C., Neff, K.-H., Nordhoff, E., and Pohlenz, H.-D. (1994) *Biochemistry 33*, 3413−3423.
15. Jagath, J. R., Sharma, B., Rao, N. A., and Savithri, H. S. (1997) *J. Biol. Chem. 272*, 24355−24362.
16. Ploux, O., and Marquet, A. (1996) *Eur. J. Biochem. 236*, 301−308.
17. Gong, J., Hunter, G. A., and Ferreira, G. C. (1998) *Biochemistry 37*, 3509−3517.
18. Hunter, G. A., and Ferreira, G. C. (1999) *Biochemistry 38*, 3711−3718.
19. Sambrook, J., Fritsch, E. F., and Maniatis, T. (1989) *Molecular Cloning: A Laboratory Manual*, 2nd ed., Cold Spring Harbor Laboratory Press, Cold Spring Harbor, NY.
20. Bradford, M. M. (1976) *Anal. Biochem. 72*, 248−254.
21. Ploux, O., and Marquet, A. (1992) *Biochem. J. 283*, 327−331.
22. Leir, C. M. (1972) *J. Org. Chem. 37*, 887−889.
23. Barney, L. C., Huber, E. W., and McCarthy, J. R. (1990) *Tetrahedron Lett. 31*, 5547−5550.
24. Hunter, G. A., and Ferreira, G. C. (1995) *Anal. Biochem. 226*, 221−224.
25. Ferreira, G. C., and Dailey, H. A. (1993) *J. Biol. Chem. 268*, 584−590.

26. Fanica-Gaignier, M., and Clement-Metral, J. (1973) *Eur. J. Biochem. 40*, 19−24.
27. Ploux, O., Breyne, O., Carillon, S., and Marquet, A. (1999) *Eur. J. Biochem. 259*, 63−70.
28. Metzler, C. M., Viswanath, R., and Metzler, D. E. (1991) *J. Biol. Chem. 266*, 9374−9381.
29. McPhalen, C. A., Vincent, M. G., and Jansonius, J. N. (1992) *J. Mol. Biol. 225*, 495−517.
30. Yano, T., Mizuno, T., and Kagamiyama, H. (1993) *Biochemistry 32*, 1810−1815.
31. Metzler, D. E., Ikawa, M., and Snell, E. E. (1954) *J. Am. Chem. Soc. 76*, 648−652.
32. Dunathan, H. C. (1966) *Proc. Natl. Acad. Sci. U.S.A. 55*, 712−716.
33. Tagaki, W., and Westheimer, F. (1968) *Biochemistry 7*, 891−901.

BI991620J